

## Pion and Kaon Polarizabilities at CERN COMPASS

MURRAY MOINSTER<sup>1</sup>

FOR THE COMPASS COLLABORATION

*R. and B. Sackler Faculty of Exact Sciences,  
School of Physics and Astronomy, Tel Aviv University,  
69978 Tel Aviv, Israel  
murraym@tauphy.tau.ac.il*

Abstract:

### Objective:

The electric ( $\bar{\alpha}$ ) and magnetic ( $\bar{\beta}$ ) pion Compton polarizabilities characterize the pion's deformation in the electromagnetic field of the  $\gamma$  during  $\gamma\pi$  Compton scattering. They depend on the rigidity of the pion's internal structure as a composite particle. The polarizabilities deduced by Antipov et al. in their low statistics Primakoff experiment ( $\sim 7000$  events) were  $\bar{\alpha}_\pi = -\bar{\beta}_\pi = 6.8 \pm 1.4 \pm 1.2$ , in units of  $10^{-43} \text{ cm}^3$ . This value, ignoring the large error bars, is about three times larger than the chiral perturbation theory ( $\chi$ PT) prediction. Taking into account the very high beam intensity, fast data acquisition, high acceptance and good resolution of the CERN COMPASS experiment, one can expect from COMPASS statistics a factor 6000 higher, a data sample that includes many tests to control systematic errors, and a significantly reduced total measurement uncertainty for  $\bar{\alpha}_\pi$ , of order 0.4.

### Methodology:

CERN COMPASS studies of pion-photon interactions, to achieve a unique Primakoff physics program centered on pion polarizability studies. We use 100-200 GeV pion beams and a virtual photon target, and magnetic spectrometers and calorimeters to measure the complete kinematics of pion-photon reactions. COMPASS was set up during 2000/01, including a successful Primakoff test run, and then began data taking with a muon beam for the proton spin physics component of its program. COMPASS will next run its spin physics program and Primakoff program preparations, followed by its pion beam physics program, including pion polarizability. For pion polarizability,  $\gamma\pi$  scattering will be measured via radiative pion scattering (pion Bremsstrahlung) in the nuclear Coulomb field:  $\pi + Z \rightarrow \pi' + \gamma + Z$ . A virtual photon from the Coulomb field of the target nucleus is scattered from the pion and emerges as a real photon accompanying the pion at small forward angles in the laboratory frame, while the target nucleus (in the ground state) recoils with a small transverse momentum kick  $p_t$ . The radiative pion scattering reaction is equivalent to  $\gamma + \pi \rightarrow \gamma + \pi$  scattering for laboratory  $\gamma$ 's of order 1 GeV incident on a target  $\pi$  at rest. The pion polarizabilities are determined by their effect on the shape of the measured  $\gamma\pi$  Compton scattering angular distribution.

### Significance:

The pion polarizabilities are key observables, and provide stringent tests of our understanding of chiral symmetry, its spontaneous breakdown, the role of explicit symmetry breaking in QCD, and consequently the very foundations of nuclear physics. The  $\chi$ PT effective Lagrangian, using data from radiative pion beta decay, predicts the pion electric and magnetic polarizabilities  $\bar{\alpha}_\pi = -\bar{\beta}_\pi = 2.7 \pm 0.4$ . New high precision pion polarizability measurements via radiative pion scattering data from COMPASS will provide important new tests of this QCD chiral dynamics prediction.

---

<sup>1</sup>together with: F. Balestra, R. Bertini, M.P. Bussa, M. Colantoni, O. Denisov, A. Dolgoplov, M. Faessler, A. Ferrero, L. Ferrero, J. Friedrich, V. Frolov, R. Garfagnini, N. Grasso, V. Kolossov, R. Kuhn, A. Maggiora, M. Maggiora, A. Manara, Y. Mikhailov, V. Obraztsov, A. Olchevski, D. Panzneri, S. Paul, G. Piragino, J. Pochodzalla, V. Poliakov, A. Sadovski, M. Sans, L. Schmitt, H. Siebert, A. Skachkova, T. Walcher, A. Zvyagin

# 1 Scientific Background:

Pion polarizabilities will be measured at the CERN COMPASS experiment [1, 2, 3, 4, 5, 6, 7, 8], a new high priority approved spectrometer facility at CERN that uses muon and pion beams for studies of hadron structure and spectroscopy. The polarizabilities are obtained from measurements of the  $\gamma\pi \rightarrow \gamma\pi$  gamma-pion Compton scattering. For the pion, chiral perturbation theory ( $\chi$ PT) leads to precision predictions for the polarizabilities [9, 10, 11, 12]. Precision measurements of polarizabilities therefore subject the  $\chi$ PT techniques of QCD to new and serious tests. The polarizability measurements described here are a part of the global COMPASS Primakoff program [2, 3, 4] to study pion and Kaon polarizabilities, chiral anomalies, and pionic and kaonic Hybrid mesons. The global COMPASS physics program was described Sept. 2002 at a CERN COMPASS Future workshop [13].

## 1.1 Pion Polarizabilities via Primakoff Scattering

For the pion polarizability,  $\gamma\pi$  scattering was measured (with large uncertainties) with 40 GeV pions [14] via radiative pion scattering (pion Bremsstrahlung) in the nuclear Coulomb field:

$$\pi + Z \rightarrow \pi' + \gamma + Z'. \quad (1)$$

In this measurement, the incident pion Compton scatters from a virtual photon in the Coulomb field of a nucleus of atomic number  $Z$ ; and the final state  $\gamma$  and pion are detected in coincidence. The radiative pion scattering reaction is equivalent to  $\gamma + \pi^- \rightarrow \gamma + \pi^-$  scattering for laboratory  $\gamma$ 's of order 1 GeV incident on a target  $\pi^-$  at rest. It is an example of the well tested Primakoff formalism [15, 16] that relates processes involving real photon interactions to production cross sections involving the exchange of virtual photons.

In the 40 GeV radiative pion scattering experiments, it was shown experimentally [14] and theoretically [17] that the Coulomb amplitude clearly dominates, and yields sharp peaks in  $t$ -distributions at very small squared four momentum transfers ( $t$ ) to the target nucleus  $t \leq 6 \times 10^{-4} \text{ (GeV/c)}^2$ . Backgrounds from strong processes were low, and are expected to be even lower at the higher energy ( $\sim 190 \text{ GeV}$ ) planned for the CERN COMPASS experiment.

**All polarizabilities in this paper are expressed in units of  $10^{-43} \text{ cm}^3$ .** The  $\chi$ PT 1-loop prediction [9, 10] for the pion polarizability is  $\bar{\alpha}_\pi = -\beta_\pi = 2.7 \pm 0.4$ ; with values  $\bar{\alpha}_\pi = 2.4 \pm 0.5$ ;  $\beta_\pi = -2.1 \pm 0.5$  at two-loop [10]. Holstein [9] showed that meson exchange via a pole diagram involving the  $a_1(1260)$  resonance provides the main contribution ( $\bar{\alpha}_\pi = 2.6$ ) to the polarizability. Xiong, Shuryak, Brown (XSB) [18] assuming  $a_1$  dominance find  $\bar{\alpha}_\pi = 1.8$ . Many other QCD based polarizability calculations, including lattice QCD [19], are also available, as described in different polarizability articles [2, 11, 20]. In this report, we emphasize comparisons with model independent chiral perturbation predictions. But we will of course compare the data to all theoretical predictions.

For the kaon, the lowest order  $\chi$ PT prediction [2, 9, 21] is  $\bar{\alpha}_{K^-} = 0.5$ . The kaon polarizability measurements at COMPASS should complement those for pion polarizabilities for chiral symmetry tests away from the chiral limit. More extensive studies of kaon polarizabilities were given in Ref. [22, 23]. Until now, only an upper limit [24] at 90% confidence was measured (via energy shifts in heavy  $Z$  kaonic atoms) for the  $K^-$ , with  $\bar{\alpha}_K \leq 200$ . Kaon polarizability measurements have never been carried out. For the kaon polarizability, due to the lower beam intensity, the statistics will be roughly 50 times less than for the pion case. But COMPASS would still obtain the first ever Kaon polarizability measurement.

## 1.2 Pion Polarizabilities

For the  $\gamma$ - $\pi$  interaction at low energy, chiral perturbation theory ( $\chi$ PT) provides a rigorous way to make predictions; because it stems directly from QCD and relies only on the solid assumptions of

spontaneously broken  $SU(3)_L \times SU(3)_R$  chiral symmetry, Lorentz invariance and low momentum transfer. Unitarity is achieved by adding pion loop corrections to lowest order, and the resulting infinite divergences are absorbed into physical (renormalized) coupling constants  $L_i^r$  (tree-level coefficients in  $L^{(4)}$ , see Refs. [25, 26]). With a perturbative expansion of the effective Lagrangian limited to terms quartic in the momenta and quark masses ( $O(p^4)$ ), the method establishes relationships between different processes in terms of the  $L_i^r$ . For example, the radiative pion beta decay and electric pion polarizability are expressed as [26]:

$$h_A/h_V = 32\pi^2(L_9^r + L_{10}^r); \bar{\alpha}_\pi = \frac{4\alpha_f}{m_\pi F_\pi^2}(L_9^r + L_{10}^r); \quad (2)$$

where  $F_\pi = 93.1$  MeV [27] is the pion decay constant,  $h_A$  and  $h_V$  are the axial vector and vector coupling constants in the decay, and  $\alpha_f$  is the fine structure constant. The experimental ratio [27]  $h_A/h_V = 0.45 \pm 0.06$ , leads to  $\bar{\alpha}_\pi = -\bar{\beta}_\pi = 2.7 \pm 0.4$ , where the error shown is due to the uncertainty in the  $h_A/h_V$  measurement [11, 12]. For the Kaon polarizability, Eq. 2 is used with the Kaon mass instead of the pion mass.

The pion polarizabilities deduced by Antipov et al. [14] in their low statistics experiment ( $\sim 7000$  events) were  $\bar{\alpha}_\pi = -\bar{\beta}_\pi = 6.8 \pm 1.4 \pm 1.2$ , with the analysis constraint that  $\bar{\alpha}_\pi + \bar{\beta}_\pi = 0$ , as expected theoretically [9]. The deduced polarizability value, not counting the large error bars, is some three times larger than the  $\chi$ PT prediction. **The available polarizability results have large uncertainties. There is a clear need for new and improved radiative pion scattering data.**

### 1.3 Meson Radiative Transitions

COMPASS will also study Primakoff radiative transitions leading from the pion to the  $\rho^-$ ,  $a_1(1260)$ , and  $a_2(1320)$ ; and for the kaon to  $K^*$ . The  $\rho$  data is obtained with the  $\gamma\pi$  polarizability trigger, while the others require a particle multiplicity trigger [4], as discussed later in Section 3.3. Radiative transition widths are predicted by vector dominance and quark models. Independent and higher precision data for these and higher resonances would be valuable as a check of the COMPASS apparatus and in order to allow a more meaningful comparison with theoretical predictions. For example, the  $\rho \rightarrow \pi\gamma$  width measurements [15, 28, 29] range from 60 to 81 keV; the  $a_1(1260) \rightarrow \pi\gamma$  width measurement ([16]) is  $0.64 \pm 0.25$  MeV; and the  $a_2(1320) \rightarrow \pi\gamma$  width is  $\Gamma = 295 \pm 60$  keV [30] and  $\Gamma = 284 \pm 25 \pm 25$  keV [31]. For  $K^* \rightarrow K\gamma$ , the widths obtained previously are  $48 \pm 11$  keV [32] and  $51 \pm 5$  keV [33].

According to Holstein [9] and XSB [18], the  $a_1(1260)$  width and the pion polarizability are related to one another. For  $a_1(1260) \rightarrow \pi\gamma$ , the experimental width [16] is  $\Gamma = 0.64 \pm 0.25$  MeV. XSB [18] used an estimated radiative width  $\Gamma = 1.4$  MeV, higher than the experimental value [16], as determined in the Primakoff reaction  $\pi Z \rightarrow a_1 Z$ , followed by  $a_1^- \rightarrow \pi^- \rho$ . It is with this estimated width that they calculate the pion polarizability to be  $\bar{\alpha}_\pi = 1.8$ . COMPASS will experimentally check the  $a_1$  assumptions of XSB via the Primakoff reaction  $\pi Z \rightarrow a_1 Z$ , and the consistency of the expected relationship of this radiative width and the pion polarizability [34].

## 2 Research Goals and Expected Significance:

We studied the statistics attainable and uncertainties achievable for the pion polarizabilities in the COMPASS experiment, based on Monte Carlo simulations. We begin with an estimated  $\sigma(Pb) = 0.5mb$  Compton scattering cross section per Pb nucleus and a total inelastic cross section per Pb nucleus of 0.8 barn. High statistics will allow systematic studies, with fits carried out for different regions of photon energy  $\omega$ ,  $Z^2$ , etc.; and polarizability determinations with statistical uncertainties lower than 0.1.

We consider a pion beam flux of  $2 \times 10^7$  pions/sec, with a spill structure that provides a 5 second beam every 16 seconds. For pion polarizability, in 2 months of running at 100% efficiency,

we obtain  $3.2 \times 10^{13}$  beam pions. We use a 0.8 % interaction length target, 3 mm Lead plate with target density  $N_t = 10^{22} \text{ cm}^{-2}$ . The Primakoff interaction rate is then  $R = \sigma(Pb) \cdot N_t = 5. \times 10^{-6}$ . Therefore, in a 2 month run, one obtains  $1.6 \times 10^8$  Primakoff polarizability events at 100% efficiency. Considering efficiencies for tracking (92%),  $\gamma$  detection (58%), accelerator and COMPASS operation (60%), analysis cuts to reduce backgrounds (75%), we estimate a global efficiency of  $\epsilon(\text{total})=24\%$ , or  $4. \times 10^7$  useful pion polarizability events per 2 month run. Prior to the data production run, time is also needed to calibrate ECAL2, to make the tracking detectors operational, to bring the DAQ to a stable mode, and for other contingencies. The above expected statistics in a two month data production run is a factor 6000 higher than the 7000 events of the previous pion polarizability Primakoff experiment.

We will also access kaon polarizabilities considering the approximately 2% kaon component of the beam. We will use the CERN CEDAR Cherenkov beam detector for the kaon particle identification. Statistics of order  $4. \times 10^5$  events would allow a first time determination of the kaon polarizability.

COMPASS provides a unique opportunity to investigate pion and Kaon polarizabilities. Taking into account the very high beam intensity, fast data acquisition, high acceptance and good resolution of the COMPASS setup, one can expect from COMPASS the highest statistics and a 'systematics-free' data sample that includes many tests to control possible systematic errors.

### 3 Detailed description of Research Program:

COMPASS is a fixed target experiment which runs primarily with a 160 GeV polarized muon beam and a 190 GeV pion beam. In order to achieve a good energy resolution within a wide energy range, COMPASS is designed as a two stage spectrometer with 1.0 Tm and 5.2 Tm conventional magnets. The tracking stations are composed of different detector types to cover a large area while achieving a good spatial resolution in the vicinity of the beam. Most of the tracking detectors operate on the principle of gas amplification, while some are silicon strip detectors. At the end of each stage, an electromagnetic and a hadronic calorimeter detects the energies of the gammas, electrons and hadrons. The calorimeters of the first stage and the EM calorimeter of the second stage have holes through which the beam passes.

We considered elsewhere in detail the beam, detector, target, and trigger requirements for polarizability studies in the CERN COMPASS experiment [2, 3, 4]. We describe these studies briefly below. The Sept. 2002 status of the COMPASS apparatus is described in Ref. [13].

#### 3.1 Monte Carlo Simulations

The setup we used for the Monte Carlo simulations was the official setup for the year 2001 run with the addition of three GEM stations and six silicon stations as projected for the year 2002 run. The additional detectors allow more precise tracking. We carried out the polarizability simulations using (1) the POLARIS event generator with (2) the CERN COMPASS GEANT (COMGEANT) package [35], whose output is a ZEBRA file with the information on the traces left by particles in detectors, (3) the CORAL COMPASS reconstruction and analysis library, structured as a set of modules: an input package is used to read the ZEBRA files produced by COMgeant, TraFiC(TRAck Finding and Fitting in Compass), calorimeter and RICH packages, a ROOT output package, the detector data decoding package, etc., and (4) the new CERN histogramming and display and fit program ROOT. We use the terms *generated* and *reconstructed*, the first denoting the input physics events to COMgeant from POLARIS and the latter the output of CORAL which contains the reconstruction of these events in the COMPASS spectrometer.

POLARIS produces events of the type Eq. 1, based on the theoretical Primakoff  $\gamma\pi$  Compton scattering cross section. The four-momentum of each particle is  $p_1, p_2, p_1', p_2', k, k'$ , respectively,

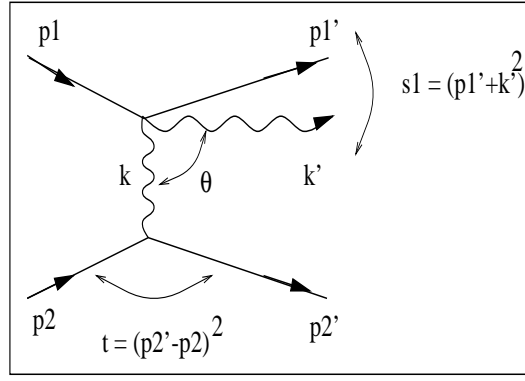


Figure 1: The Primakoff  $\gamma$ -hadron Compton process and kinematic variables (4-momenta):  $p1, p1'$  = for initial/final hadron,  $p2, p2'$  = for initial/final target,  $k, k'$  = for initial/final gamma, and  $\theta$  the scattering angle of the  $\gamma$  in the alab frame.

as shown in Fig. 1. In the one-photon exchange domain, this reaction is equivalent to  $\gamma + \pi \rightarrow \gamma' + \pi'$ , and the four-momentum of the incident virtual photon is  $k = q = p2 - p2'$ . We have therefore  $t = k^2$  with  $t$  the square of the four-momentum transfer to the nucleus,  $F(t)$  the nuclear form factor (essentially unity at small  $t$ ,  $\sqrt{s}$  the mass of the  $\gamma\pi$  final state, and  $t_0$  the minimum value of  $t$  to produce a mass  $\sqrt{s}$ . The momentum modulus  $|\vec{k}|$  (essentially equal to  $p_T$ ) of the virtual photon is in the transverse direction, and is equal and opposite to the momentum  $p_T$  transferred to the target nucleus. The pion polarizability is extracted via a fit of the theoretical cross section to the scattered  $\gamma$  angular distribution in the projectile (alab) rest frame. The total Primakoff cross section is computed by integrating numerically the differential cross section  $\sigma(s, t, \theta)$  of Eq. 3 below for the Primakoff Compton process.

### 3.2 Primakoff $\gamma\pi$ Compton Event Generator

We describe the event generator for the radiative scattering of the pion in the Coulomb field of a nucleus [21]. In the pion alab frame, the nuclear Coulomb field of target  $M_Z$  effectively provides a virtual photon beam incident on a pion target at rest. We have for the variable  $t = k^2 = q^2 \equiv M^2$ , where  $t$  is the 4-momentum transferred to the nucleus, and  $M$  is the virtual photon mass. Since  $t = 2M_Z[M_Z - E(Z', \text{lab})] < 0$ , the virtual photon mass is imaginary. To approximate real pion Compton scattering, the virtual photon should be taken to be almost real. For small  $t$ , the electromagnetic contribution to the scattering amplitude is large compared to meson and Pomeron (diffractive) exchange contributions. Radiative corrections for Primakoff scattering have been calculated to be very small [36].

The Primakoff differential cross section of the process of Eq. 1 in the alab frame may be expressed as [37]:

$$\frac{d^3\sigma}{dt d\omega d\cos\theta} = \frac{\alpha_f Z^2}{\pi\omega} \cdot \frac{t - t_0}{t^2} \cdot \frac{d\sigma_{\gamma\pi}(\omega, \theta)}{d\cos\theta} \cdot F^2(t), \quad (3)$$

where the  $\gamma\pi$  cross section is given by:

$$\frac{d\sigma_{\gamma\pi}(\omega, \theta)}{d\cos\theta} = \frac{2\pi\alpha_f^2}{m_\pi^2} \cdot \left\{ F_{\gamma\pi}^{pt}(\theta) + \frac{m_\pi\omega^2}{\alpha_f} \cdot \frac{\bar{\alpha}_\pi(1 + \cos^2\theta) + 2\bar{\beta}_\pi\cos\theta}{\left(1 + \frac{\omega}{m_\pi}(1 - \cos\theta)\right)^3} \right\}. \quad (4)$$

Here,  $t_0 = (m_\pi\omega/p_b)^2$ , with  $p_b$  the incident pion beam momentum in the laboratory,  $\theta$  the scattering angle of the real photon relative to the incident virtual photon direction in the alab frame,  $\omega$  the energy of the virtual photon in the alab frame,  $Z$  the nuclear charge,  $m_\pi$  the pion mass,  $\alpha_f$  the fine structure constant,  $F(t)$  is the nuclear electromagnetic form factor (approximately unity in the

range  $t < 2.5 \times 10^{-4} \text{GeV}^2$ ), and  $\bar{\alpha}_\pi, \bar{\beta}_\pi$  the pion electric and magnetic polarizabilities. The energy of the incident virtual photon in the alab (pion rest) frame is:

$$\omega \sim (s - m_\pi^2)/2m_\pi. \quad (5)$$

For COMPASS, this radiative pion scattering reaction is then equivalent to  $\gamma + \pi \rightarrow \gamma + \pi$  scattering for laboratory  $\gamma$ 's with energy of order  $\omega = 1 \text{GeV}$  incident on a target  $\pi$  at rest. The function  $F_{\gamma\pi}^{pt}(\theta)$  describing the Thomson cross section for  $\gamma$  scattering from a point pion is given by:

$$F_{\gamma\pi}^{pt}(\theta) = \frac{1}{2} \cdot \frac{1 + \cos^2\theta}{\left(1 + \frac{\omega}{m_\pi}(1 - \cos\theta)\right)^2}. \quad (6)$$

From Eq. 4, the cross section depends on  $(\bar{\alpha}_\pi + \bar{\beta}_\pi)$  at small  $\theta$ , and on  $(\bar{\alpha}_\pi - \bar{\beta}_\pi)$  at large  $\theta$ . A precise fit of the theoretical cross section (Eq. 3-6) to the measured angular distribution of scattered  $\gamma$ 's, allows one to extract the pion electric and magnetic polarizabilities. Fits will be done for different regions of  $\omega$  for better understanding of the systematic uncertainties. We will carry out analyses with and without the dispersion sum rule constraint [9] that  $\bar{\alpha}_\pi + \bar{\beta}_\pi \approx 0.4$ . We can achieve a significantly smaller uncertainty for the polarizability by including this constraint in the fits.

The event generator produces events in the alab frame, characterized by the kinematic variables  $t$ ,  $\omega$  and  $\cos\theta$ , and distributed with the probability of the theoretical Compton Primakoff cross section (Eq. 3-6). Then, the  $\gamma\pi$  scattering kinematics are calculated. The virtual photon incident along the recoil direction  $\vec{k}/|\vec{k}|$ , is scattered on the pion "target", and emerges as a real photon with energy/momentum  $\omega'/|\vec{k}'|$  at an angle  $\theta$ :

$$\omega' = \frac{\omega\left(1 + \frac{\omega^2 - |\vec{k}|^2}{2m_\pi\omega}\right)}{1 + \frac{\omega}{m_\pi}\left(1 - \frac{|\vec{k}|}{\omega} \cos\theta\right)} \quad (7)$$

The photon azimuthal angle around the recoil direction is randomly generated using a uniform distribution. The four-vector components of all reaction participants (pion, photon and recoil nucleus) are then calculated in the alab frame. The azimuthal angle of the recoil nucleus is also randomly generated by a uniform distribution. Finally, the reaction kinematics are transformed to the lab frame by a Lorentz boost.

For the measurement of the pion polarizabilities, one must fit the theoretical cross section (3-6) to measured distributions, after correcting for acceptances. The sensitivity to the polarizability increases with increasing  $\omega$  energy and at back angles. A convenient method is to use the  $\cos\theta$  distribution integrated over  $t$  and for different ranges of  $\omega$ , since this shows clearly the sensitivity to the polarizability.

### 3.3 Design of the Primakoff Trigger

The small Primakoff cross section and the high statistics required for extracting polarizabilities require a data run at high beam intensities and with good acceptance. This sets the main requirements for the trigger system: (1) to act as a "beam killer" by accepting only Primakoff scattered pions, and suppressing the high rate background associated with non-interacting beam pions, (2) to avoid cutting the acceptance at the important  $\gamma$  back angles in the alab frame, where the hadron polarizability measurement is most sensitive, (3) to cope with background in the  $\gamma$  calorimeter from low energy  $\gamma$ 's or delta electrons.

We achieve these objectives via a COMPASS Primakoff trigger that makes use of a beam veto, a target recoil detector, the calorimeters and various hodoscopes. A coincidence is required of the

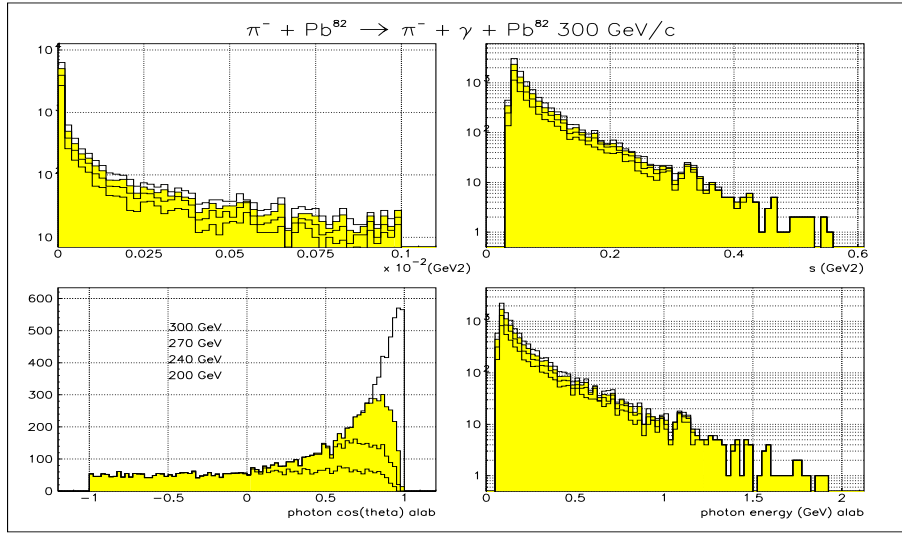


Figure 2: MC simulation showing the acceptance of the  $\gamma\pi \rightarrow \gamma\pi$  reaction in terms of the invariant four momentum transfer  $t$  to the target, the squared invariant energy  $s$  of the final state  $\gamma\pi$ , the angular distribution versus  $\cos(\theta)$  with  $\theta$  the  $\gamma$  scattering angle in the alab frame, and the virtual photon energy  $\omega$  in the alab frame. The overlaid spectra correspond to different cuts on the final state  $\pi$  momentum.

scattered pion with a  $\gamma$  measured in the ECAL2 calorimeter. We demonstrated the feasibility and field operation of such a trigger, via Monte Carlo simulations [2, 3, 4, 5, 6, 7] and via beam tests with the COMPASS spectrometer [38].

For the reaction given in Eq. 1, for illustration at 300 GeV pion beam energy, the laboratory outgoing  $\gamma$ 's are emitted within an angular cone of within 5 mrad, and the corresponding outgoing  $\pi$ 's are emitted within 2 mrad. Most events have  $\gamma$  energies between 0 – 280 GeV, and  $\pi$  energies between 20 – 300 GeV.

Our MC shows that we lose very little polarizability information by applying an “energy cut” trigger condition that rejects events with the outgoing pion energy having more than 240 GeV. Correspondingly, the final state  $\gamma$  has less than 60 GeV. The 240 GeV cut acts as a beam killer. The 60 GeV cut will also be very effective in reducing the  $\gamma$  detector (ECAL2) trigger rate, since a large part of the background  $\gamma$  rate is below 60 GeV.

The polarizability insensitivity to these cuts results from the fact that the most forward (in alab frame) Compton scattering angles have the lowest laboratory  $\gamma$  energies and largest laboratory angles. In addition, the cross section in this forward alab angle range is much less sensitive to the polarizabilities. This is seen from Eq. 4, since with  $\bar{\alpha}_\pi + \bar{\beta}_\pi \approx 1$  used in our MC, the polarizability component is small at forward compared to back angles. The acceptance is reduced by the energy cut for the forward alab angles (shown in Fig. 2), but is unaffected at the important alab back angles. Summarizing, the pion and  $\gamma$  energy constraints at the trigger level fulfill the “beam killer” requirement and at the same time remove backgrounds coming from low energy  $\gamma$ 's, delta electrons, and  $e^+e^-$  pairs incident on ECAL2, etc. Similar results are obtained for the effectiveness of an energy loss trigger for simulations carried out at 190 GeV pion beam energy.

Test beam studies for the trigger were performed in Sept. 2000 [38]. The setup for the test beam was the following (see Fig. 3): a beam counter upstream of the target (S); a beam veto counter (beam killer) in front of ECAL2, covering the hole for the deflected primary beam (B); a hodoscope 80 cm  $\times$  96 cm, situated in front of ECAL2 (H), displaced horizontally by 20 cm from the position of the deflected beam; a veto system around the target and the electromagnetic calorimeter (ECAL2).

According to the signature of the reaction, a beam particle is expected in S. Particles scattered

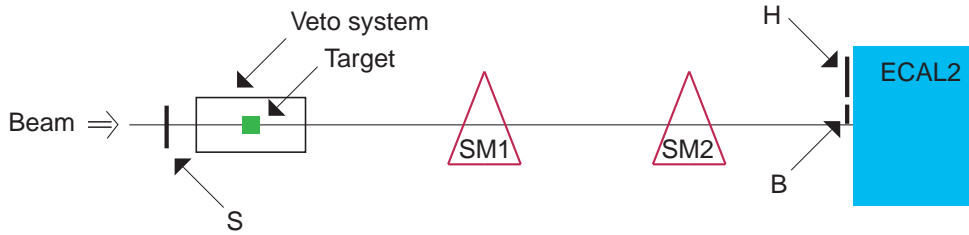


Figure 3: Trigger setup for the Primakoff measurement in COMPASS. It consists of a beam counter (S), beam veto counter (B), a hodoscope (H), a veto system around the target and the electromagnetic calorimeter (ECAL2).

by the target, should give a signal in H. No signal should be registered in the beam killer B, but a highly energetic photon should be detected in ECAL2. The test beam demonstrated that an acceptable rate for the trigger can be achieved. The requirements to achieve this rate are the following: the coincidence between the energy deposition in the ECAL2 above a threshold of  $0.2$  to  $0.3 \times E_{beam}$  and the existence of a charged particle in the corresponding acceptance of H. The use of the beam killer B and of the veto counter does not improve much the rate reduction. The target veto could be used offline to reject background reactions with large momentum transfer to the target.

Some interesting numbers that are quoted include the following: from a beam intensity of  $6 \cdot 10^6$ /spill with a 3 mm lead target, the trigger rate was found to be  $2.5 \times 10^5$ /spill. The trigger gives a reduction factor of 24. The idea of the trigger is not to reduce too strongly the number of events since this will be done offline when analysing the events. The size of the hodoscope needed to cover the acceptance of the simulated scattered pions was calculated by plotting the simulated hit distribution of the scattered pions at the position where the hodoscope will be situated. Fig. 4 shows that the size needed for the hodoscope is 1 meter in horizontal direction and 40 cm. in vertical direction.

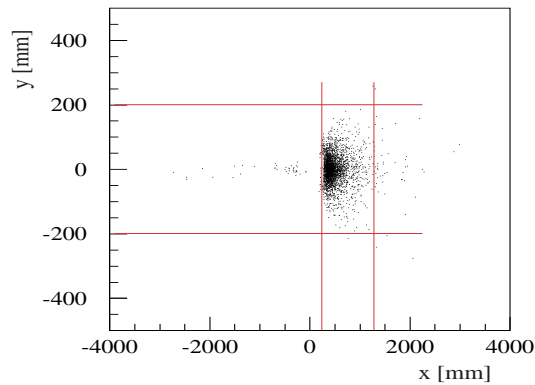


Figure 4: Simulated hit distribution of the scattered pion at 30 meters from the target. The lines indicate the possible size of the trigger hodoscope.

Aside from the polarizability trigger discussed above, COMPASS will implement as well a meson radiative transition trigger. The trigger uses the characteristic decay pattern: one or three charged mesons with gamma hits, or three charged mesons and no gamma hits. The trigger [3, 4] is based on a determination of the pion energy loss (via its characteristic angular deflection), correlated in downstream scintillator hodoscope stations (H1 versus H2) with the aid of a fast matrix chip, as shown in Fig. 5. This trigger is a copy of the currently running muon beam energy loss trigger [13]. We will use the Beam Kill veto trigger detectors BK1/BK2 only for low intensity tests. They follow the pion trajectory, as shown in Fig. 5, but they can not handle the full 100 MHz beam rate.



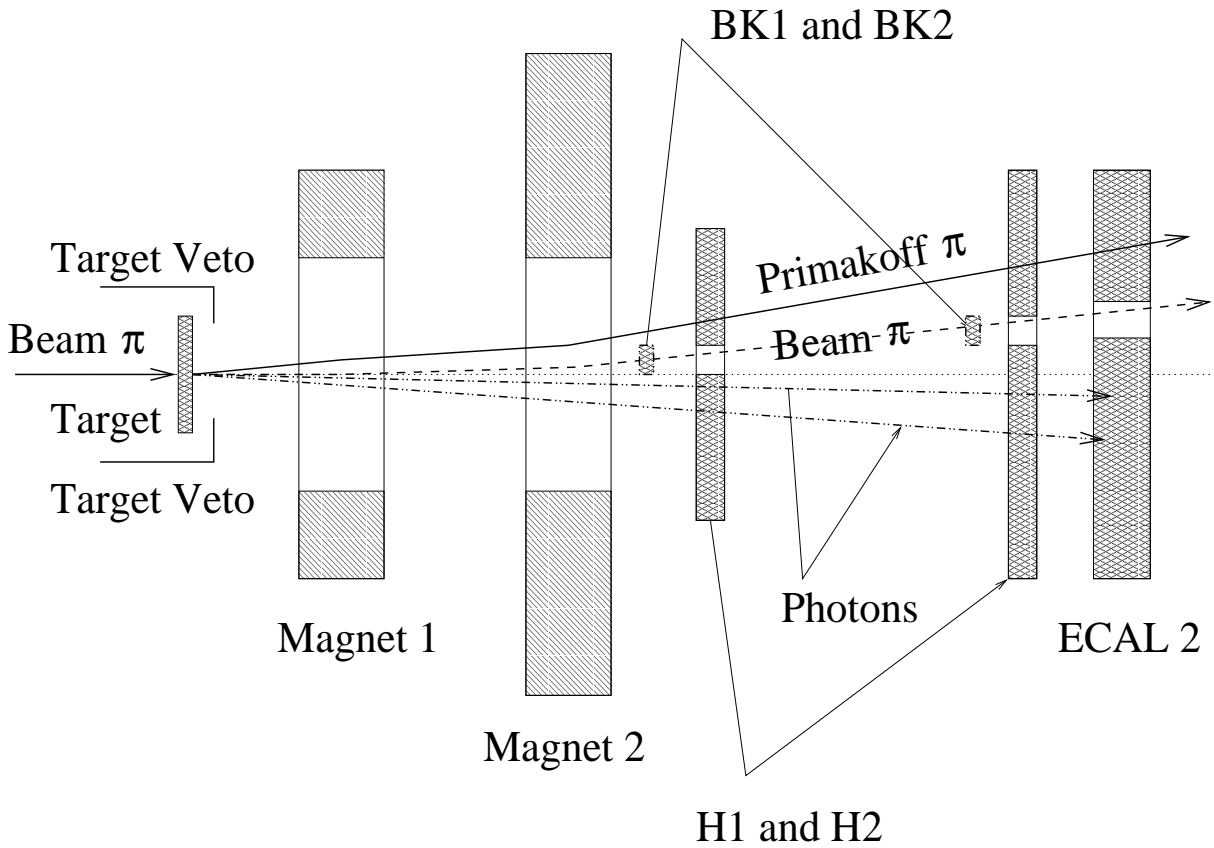


Figure 5: Detector layout for the COMPASS Primakoff Hybrid trigger,  $\pi^- Z \rightarrow \text{Hybrid} \rightarrow \pi^- \eta$ . BK1,BK2=beam killer system, H1,H2=hodoscope system for charged particle detection, ECAL2=second photon calorimeter. For  $\eta$  decay, one observes the two  $\gamma$ s shown. For polarizability, there is only one  $\gamma$  to detect.

### 3.4 Beam Requirements

In COMPASS, two beam Cherenkov detectors (CEDAR) far upstream of the target provide  $\pi/K/p$  particle identification (PID). The incoming hadron momentum is measured in the beam spectrometer. Before and after the target, charged particles are tracked by high resolution silicon tracking detectors. The measurement of both initial and final state momenta provides constraints to identify the reaction. The final state pion and  $\gamma$  momenta are measured downstream in the magnetic spectrometer and in the  $\gamma$  calorimeter, respectively. These measurements allow a precise determination of the small  $p_T$  kick to the target nucleus, the main signature of the Primakoff process, and the means to separate Primakoff from meson exchange scattering events.

We can get quality statistics for the pion study with high beam intensities at the CERN SPS. We will take data with different beam energies and targets, with both positive and negative beams, as part of efforts to control systematic errors. We will also take data with protons (positive beam) and antiprotons (negative beam with PID) to determine the proton polarizability [39] by proton Primakoff Compton scattering, to self-calibrate our Primakoff Compton scattering methodologies.

For the 120-300 GeV hadron beams, particle identification (PID) is needed to provide pion, kaon, proton beam tag for positive and negative beams at different beam energies. For the COMPASS beam, one expects [40] a beam intensity of 100 MHz, with beam composition roughly: 120-300 GeV/c, negative, 87-98% pions, 7-1% kaons, 2%-1% antiprotons; 120-300 GeV/c, positive, 43-2% pions, 7-1% kaons, 49-97% protons. PID is accomplished at CERN with CEDAR detectors, Cherenkov Differential counter with Achromatic Ring focus. There are two CEDAR detectors (in series) in the COMPASS beamline [41]. They each have eight large area PMTs arranged in a circle, preceded by a single light diaphragm (LD) to finely fix a ring radius. For the PID, a six-fold

coincidence is required. The gas pressure is varied to set the ring radius of pions or Kaons or protons at the LD location, to choose one of the particle types. The Narrow diaphragm mounted in CEDAR-N separated kaons from pions up to 300 GeV/c and could detect protons down to 12 GeV/c.

### 3.5 Target and Target Detectors

The target platform is moveable and allows easy insertion of a normal solid state target, e. g. a cylindric lead plate 40 mm in diameter and 3 mm in width. We also plan Primakoff scattering on nuclei with  $Z < 82$  to check the expected  $Z^2$  cross section dependence, and to allow corrections for double photon exchange [36]. We use silicon tracking detectors before and immediately after the targets. These are essential for Primakoff reactions as the scattering angle has to be measured with a precision of order  $100 \mu\text{rad}$ , because it contains much of the information. We veto target break-up events by a target veto recoil detector, and by selecting low- $t$  events in the off-line analysis. The recoil detector is currently developed and tested. A particle momentum of about 100 MeV should be sufficient to trigger a veto coincidence in its scintillator and Lead glass layers. This veto will limit the angular acceptance to about 100 mrad to reject events where fragments of the nucleus or particles produced in diffractive processes leave the target with bigger angles to the beam axis.

### 3.6 The Magnetic Spectrometer and the $t$ -Resolution

We achieve good momentum resolution for the incident and final state pions and  $\gamma$ 's, and therefore good four momentum  $t$ -resolution. The relative momentum resolution for  $\pi^-$  with all interactions accounted for is 1% for energies above 35 GeV and up to 2.5% below this mark. The angular resolution in a single coordinate for a pion of momentum  $p$  is  $7.9 \text{ mrad-GeV}/p$ . All generated pions with energy greater than 2 GeV were in the acceptance of the spectrometer, the reconstruction efficiency with interactions enabled is 92%.

The angular resolution for the final state  $\pi$  is controlled by minimizing the multiple scattering in the targets and detectors. With a lead target of 1% interaction length ( $2 \text{ g/cm}^2$ , 30% radiation length), multiple Coulomb scattering (MCS) of the beam and outgoing pion in the target gives an rms angular resolution of order  $40 \mu\text{rad}$ , small compared to the intrinsic tracking detector angular resolution. The target contributes to the resolution of the transverse momentum  $p_T$  via the  $p_T$  generated through MCS. Considering  $t = p_T^2$ , including all other effects [2, 3, 4], we aim for a  $p_T$  resolution less than 15 MeV, corresponding to  $\Delta t$  better than  $\approx 2.5 \times 10^{-4} \text{ GeV}^2$ .

This resolution will allow an effective  $t$ -cut to minimize contributions to the data from diffractive processes. The goal is achievable, based on the  $t$  distributions measured at a 200 GeV low statistics, high resolution experiment for  $\pi^- Z \rightarrow \pi^- \pi^0 Z$  [15] and  $\pi^- Z \rightarrow \pi^- \gamma Z$  [16] Primakoff scattering at 200 GeV at FNAL. The  $t$  distribution of the  $\pi^- \rightarrow \pi^- \gamma$  data agrees well with the Primakoff formalism out to  $t = 10^{-3} \text{ GeV}^2$ , which indicates that the data are indeed dominated by Coulomb production. Minimum material (radiation and interaction lengths) in COMPASS will also give a higher acceptance, since that allows  $\gamma$ 's to arrive at ECAL2 with minimum interaction losses, and minimum  $e^+e^-$  backgrounds.

### 3.7 The $\gamma$ Calorimeter ECAL2

The position resolution in the second  $\gamma$  calorimeter ECAL2 for the photon is 1.0 mm corresponding to an angular resolution of  $30 \mu\text{rad}$ . In the interesting energy range the energy resolution is better than 1% after taking into account the leakage into the hadron calorimeter HCAL. The photon acceptance is 98% due to the beam hole of ECAL2 while the reconstruction efficiency is 58% as a result of pair production within the spectrometer.

This  $\gamma$  detector is equipped with 3.8 by 3.8 cm<sup>2</sup> GAMS lead glass blocks to make a total active area of order 1.5 m diameter. The central area needed for the polarizability measurement is completely instrumented with modern ADC readouts.

The  $p_T$  kicks of the COMPASS magnets are 0.45 GeV/c for SM1 (4 meters from target) and 1.2 GeV/c for SM2 (16 meters from target). The fields of both magnets are set *additive* for maximum deflection of the beam from the zero degree (neutral ray) line. We thereby attain at least 10 cm for the distance between the zero degree line and the hole edge. This is important since the Primakoff  $\gamma$ 's are concentrated around the zero degree line and a good  $\gamma$  measurement requires clean signals from 9 blocks, centered on the hit block. From MC simulations, the number of Primakoff scattered pions below 40 GeV is less than 0.3%, so that 40 GeV pions are about the lowest energy of interest.

For the precise monitoring of the energy calibration of the photon calorimeters, COMPASS will use LED and laser monitor systems, as described in Ref. [42].

The available COMPASS ECAL does not have radiation hardened blocks near the beam hole. If those will be available, it would allow increasing the beam intensity a factor of five, to allow substantially more statistics for the same run time.

## 4 Simulation Results for 190 GeV Pion Beam

The most recent COMPASS Primakoff polarizability simulation results [5, 6, 7] are given now. We evaluated the single particle detection properties of the COMPASS spectrometer. The key results are a momentum resolution for pions of 1% above 35 GeV and up to 2.5% below 35 GeV accompanied by an angular resolution of 7.9 mrad GeV/ $p$  and an energy resolution for photons of 1.5% above 90 GeV accompanied by an angular resolution of 30  $\mu$ rad. The photon reconstruction inefficiency is given by the conversion probability before leaving the second spectrometer magnet; the corresponding efficiency is 58%. The single pion reconstruction efficiency is about 92%.

We describe the results of the simulation of Primakoff Compton scattering and of hadronic backgrounds. We study the influence of the COMPASS detector resolutions and reconstruction algorithms on the extraction of the polarizabilities. We achieve this via a simulation of Primakoff Compton scattering of  $\pi^-$  on Lead at a beam energy of 190 GeV at five different pairs of  $\bar{\alpha}$  and  $\bar{\beta}$  polarizability parameters with a total statistics of five times 620,000 events, each sample corresponding to the analyzed events from roughly a day of COMPASS data taking.

The following cuts are used to recognize Primakoff events: there has to be a photon hit in the ECAL2 above a certain energy and a negative charged track which carries the complementary energy. The cut on the photon energy has to be well above the energy deposition of hadrons in the electromagnetic calorimeter that is of the order of some GeV. In order to select the so-called "hard events" with most information on the pion polarizabilities, this cut is raised to 30–50% of the beam energy. In this simulation a cut on the photon energy at 90 GeV was implemented in the generator, so it was natural to use 80 GeV in the reconstruction. The energy window for the sum of pion and photon was set to 180–196 GeV to allow for the longitudinal energy leakage of ECAL2. The figures 6-9 were all produced only with the events that were left after applying these two cuts.

The reconstructed count rates have to be corrected for the inefficiency of the detector before fitting the cross section. The data of all five samples are merged to calculate the dependence of the reconstruction efficiency on the photon energy in the laboratory frame. Fig. 6 shows the generated and—with the cuts applied—the reconstructed photon energy in the laboratory frame, Fig. 7 shows the corresponding efficiency with fit parameters. As expected from our studies of single photon and pion efficiencies, the overall efficiency is between 50-55%. Fig. 8 shows the beam energy distribution used in the simulation.

Compared to the generated  $t = q^2$  distribution, the reconstructed  $q^2$  is smeared out due to the transverse momentum transfer error induced by angle reconstruction errors of the final state.

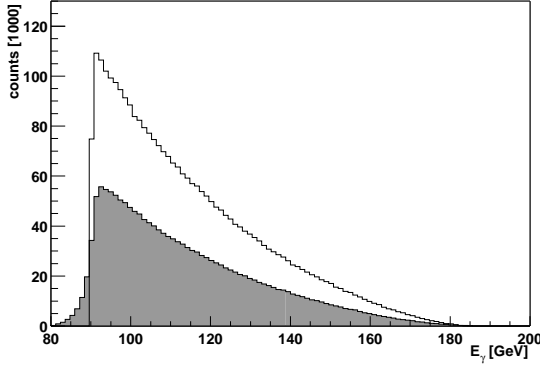


Figure 6: generated (white) and reconstructed (shaded) photon energy in the laboratory frame. The data of all five samples is merged ( $2.9 \cdot 10^6$  events)

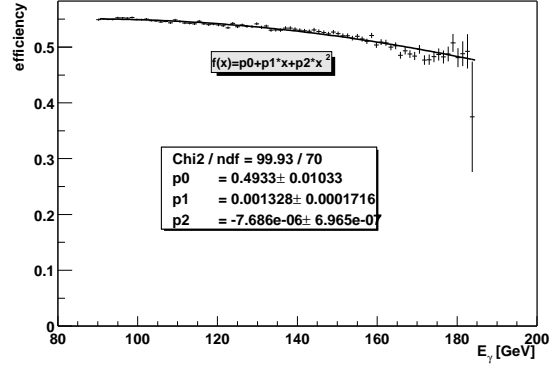


Figure 7: reconstruction efficiency vs. photon energy in the laboratory frame. The error bars are the binomial errors corresponding to the generated statistics shown in the left hand plot

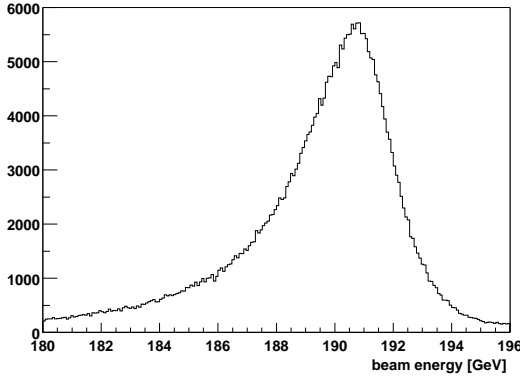


Figure 8: reconstructed beam energy

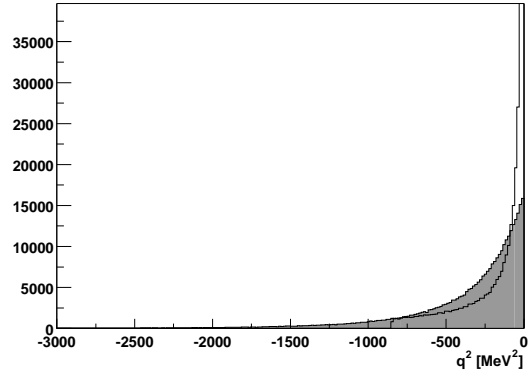


Figure 9: generated (white) and reconstructed (shaded)  $q^2$

For example, quadratically adding the errors for 110 GeV photon energy and 80 GeV pion momentum yields an error of 15 MeV. Nevertheless the rise is steep enough to permit a cut at  $-q^2 < 1000 \text{ MeV}^2$ , as seen in Fig. 9. Such a cut only reduces the efficiency by 6%.

We studied the efficiency for the selected events with small  $t$  and where the sum of the energy of the  $\pi^-$  and the  $\gamma$  is, within some resolution, equal to the energy of the beam. We found that this efficiency was independent of  $t$ , with no bias by the acceptance of the detector. Regardless of the cut in  $t$ , the important shape of the  $\gamma\pi$  angular distribution is not affected.

#### 4.1 Retrieving the polarizabilities

The generated and reconstructed four-momenta are transformed to the projectile (alab) frame. The fit is performed using the ROOT interface to the MINUIT package. To get the reconstructed differential cross section the event rates had to be corrected for the inefficiency of the detector. We observe that  $\bar{\alpha}$  and  $\bar{\beta}$  are anti-correlated, with the consequence that  $\bar{\alpha} + \bar{\beta}$  is determined with a much smaller error than  $\bar{\alpha} - \bar{\beta}$ . The polarizability effect is proportional to  $\bar{\alpha} + \bar{\beta}$  for  $\cos \theta = 1$  and  $\bar{\alpha} - \bar{\beta}$  for  $\cos \theta = -1$ , increasing with the photon energy like  $\omega^2$ . So  $\bar{\alpha} - \bar{\beta}$  is mostly determined in the region with least events while  $\bar{\alpha} + \bar{\beta}$  is better known because the cross section has a steep rise towards positive  $\cos \theta$ .

We carried out fits to determine the polarizabilities for each sample of 620,000 simulated events, each sample corresponding to different  $(\bar{\alpha}, \bar{\beta})$  pairs. Reducing the statistical errors by 8, scaling to the assumed  $4. \times 10^7$  events, we estimate the statistical uncertainties for the two month COM-PASS run to be about 0.05 for  $\bar{\alpha}$  and  $\bar{\beta}$ , 0.01 for  $\bar{\alpha} + \bar{\beta}$  and 0.1 for  $\bar{\alpha} - \bar{\beta}$ . Including systematic uncertainties, we aim to achieve better than 0.4 uncertainties in  $\bar{\alpha}$  and  $\bar{\beta}$ .

## 4.2 The hadronic background

To investigate the corruption of the measured Primakoff cross section by hadronic background events, a large sample of minimum bias events was produced with the Fritiof pion-Nucleus event generator. The analysis of  $4.5 \times 10^6$  events by the exact process described above accepts only 34 events, 27 of them were in the fit range for the polarizabilities [6].

As Fritiof only simulates hadronic interaction the mechanism for accepting some of the events is the production of  $\pi^0$  or  $\eta$ . Because of the cut on the total energy sum of the pion and the photon, most of this background is rejected, as the remaining particles also receive their part of the energy. One may tighten this cut because the background would be much more affected than the real events.

The generated final state in all 34 cases contains a nucleon. This suggests that the nucleus was disintegrated in the reaction. The fragments are tracked by COMgeant, but there is no single particle ID to label them. Thus, they unfortunately are not part of the list of particles emerging from the primary vertex. Every event contains particles with polar angles bigger than 20 deg and a target recoil would see some of those events not stopped inside the target.

The overall signal to noise ratio for hadronic background can be estimated from the ratio of the cross sections and the background suppression. The hadronic interaction length of Lead of  $194 \text{ g cm}^{-2}$  corresponds to a cross section of 1.77 barn, the suppression factor of  $26/4500000$  reduces this to  $10 \text{ } \mu\text{barn}$ . This has to be compared to the cross section of Primakoff Compton scattering—with a produced photon energy of at least 90 GeV—of about  $500 \text{ } \mu\text{barn}$ . The ratio of 50:1 will be further improved by the inclusion of the target recoil veto and by a more sophisticated kinematics reconstruction.

## 5 Other Pion Polarizability Experiments

The present proposal deals only with our experimental efforts at CERN COMPASS. But we will also compare COMPASS data to new Mainz data. At MAMI-B at Mainz, measurements [43] and calculations [44] are under way of  $p(\gamma, n\pi^+\gamma')$  radiative pion photoproduction reaction on the proton. The elastic  $\gamma\pi^+$  scattering cross section can be found by extrapolating such data to the pion pole. This corresponds to "Compton" scattering of gamma's from virtual  $\pi^+$  targets in the proton, and therefore also allows a measure of the pion polarizability. The experiment ran with 500-800 MeV tagged photons, with detection of  $\gamma'$ , neutron, and charged pion in coincidence. A similar pion polarizability experiment with polarized tagged photons was proposed [45], associated with the proposed JLab 12 GeV upgrade. Theoretical studies [44] show that the precision of this method, aside from the available statistics, is limited by the systematic errors associated with the extrapolation to the pion pole. Primakoff scattering has the advantages that meson exchange backgrounds and final state interactions are strongly suppressed. Pion polarizabilities have also been determined from two photon  $\gamma\gamma \rightarrow \pi^+\pi^-$  data [11]. However, as noted in the pion polarizability theory review of Portoles and Pennington [20]: "Knowing the low energy  $\gamma\gamma \rightarrow \pi^+\pi^-$  cross section accurately still allows large uncertainties in the polarizabilities. Only measurements of Compton scattering will resolve these." Still, intercomparisons between COMPASS and past plus new experiments [11, 43, 45], with complementary methodologies, should help fix the systematic uncertainties.

## 6 Conclusions

COMPASS is on track to measure the  $\gamma\pi$  Compton scattering cross sections, as a central part of its Primakoff physics program, thereby enabling determinations of the pion polarizabilities. The experiment will allow serious tests of  $\chi$ PT; and of different available polarizability calculations in QCD.

## 7 Acknowledgments

This research was supported in part by the Israel Science Foundation founded by the Israel Academy of Sciences and Humanities.

## References

- [1] F. Bradamante, S. Paul et al., CERN Proposal COMPASS, <http://wwwcompass.cern.ch/>, CERN/SPSLC 96-14, SPSC/P297; CERN/SPSLC 96-30, SPSC/P297, Addendum 1; <http://www-nuclear.tau.ac.il/~murraym/primaphysreps.html>
- [2] M. A. Moinester, V. Steiner, Pion and Kaon Polarizabilities and Radiative Transitions, Proc. 'Chiral Dynamics Workshop' U. Mainz, Sept. 1997, hep-ex/9801008.
- [3] M. A. Moinester, V. Steiner, S. Prakhov, Hadron-Photon Interactions in COMPASS, Proc. XXXVII Meeting on Nuclear Physics, Bormio, Italy, Jan. 1999, hep-ph/9910039
- [4] M. A. Moinester, Pion Polarizabilities and Hybrid Meson Structure at COMPASS, Contribution to the APS DNP Town Meeting on Electromagnetic & Hadronic Physics, Dec. 2000, Newport News, Va., hep-ex/0012063
- [5] M. Sans Merce, Ph.D. thesis, Ludwig Maximilians University, Munich, 2001.
- [6] R. Kuhn, Diploma thesis, Technical University, Munich, 2001.
- [7] M. Colantoni et al., Proc. XL Meeting on Nuclear Physics, Bormio, Italy, Jan. 2002.
- [8] A. Olchevski, M. Faessler, M. A. Moinester, Experimental Requirements for COMPASS Initial Primakoff Physics Program, COMPASS Collaboration Meeting presentations, 1999-2002.
- [9] B. R. Holstein, *Comments Nucl. Part. Phys.* **19**, 239 (1990).
- [10] U. Burgi, *Nucl. Phys.* B479 (1996) 392; *Phys. Lett.* B377 (1996) 147.
- [11] D. Babusci, S. Bellucci, G. Giordano, G. Matone, A. M. Sandorfi, M. A. Moinester, *Phys. Lett. B* **277**, 158 (1992).
- [12] V. Kartvelishvili, M. Margvelashvili, G. Shaw, *Nucl. Phys. Proc. Suppl.* 54A (1997) 309
- [13] CERN Workshop on Future Physics at COMPASS, Sept. 2002, Proceedings, <http://compass-cw2002.web.cern.ch/compass-cw2002/programme.htm>
- [14] Yu. M. Antipov et al., *Phys. Lett. B* **121**, 445 (1983), *Z. Phys. C* **26**, 495 (1985).
- [15] T. Jensen et al., *Phys. Rev. D* **27**, 26 (1983).
- [16] M. Zielinski et al., *Phys. Rev. Lett.* **52**, 1195 (1984); *Phys. Rev.* **29D** (1984) 2633.
- [17] A. S. Galperin et al., *Sov. Jour. Nucl. Phys.* **32**, 545 (1980).
- [18] L. Xiong, E. Shuryak, G. Brown, *Phys. Rev. D* **46**, 3798 (1992).
- [19] L. Zhou et al., MAGNETIC POLARIZABILITY OF HADRONS FROM LATTICE QCD, hep-lat/0209128; ELECTRIC POLARIZABILITY OF HADRONS, J. Christensen et al., hep-lat/0209043; W. Wilcox, CHARGED PION POLARIZABILITY FROM THE LATTICE, *Nucl. Phys. Proc. Suppl.* 53 (1997) 302, hep-lat/9607024; H. Fiebig et al., A STUDY OF HADRON ELECTRIC POLARIZABILITY IN QUENCHED LATTICE QCD, *Nucl. Phys.* B324 (1989) 47.
- [20] J. Portoles, M. R. Pennington, Theoretical Prediction of Pion Polarizabilities, DAΦNE Physics Handbook, hep-ph/9407295.
- [21] M. Buenerd, *Nucl. Instr. Meth.* A136 (1995) 128; V. Steiner, M. A. Moinester, M. Buenerd, POLARIS, A Monte Carlo event generator for polarizability experiments, 1995, unpublished.
- [22] D. Ebert, M. K. Volkov, *Phy. Atom. Nucl.* **60**, 796 (1997).

- [23] F. Guerrero, J. Prades, *Phys. Lett.* 405B (1997) 341.
- [24] G. Backenstoss et al., *Phys. Lett. B* **43**, 431 (1973).
- [25] J. Gasser and H. Leutwyler, *Nucl. Phys. B* **250**, 465 (1985).
- [26] J. F. Donoghue, B. R. Holstein, *Phys. Rev. D* **40**, 2378 (1989).
- [27] Particle Data Group, G. P. Yost et al., *Phys. Lett. B* **204**, 1 (1988);  
L. Montanet et al., *Phys. Rev. D* **50**, 1173 (1994).
- [28] J. Huston et al., *Phys. Rev.* **33** (1986) 3199.
- [29] L. Capraro et al., *Nucl. Phys.* **B288** (1987), 659.
- [30] S. Cihangir et al., *Phys. Lett.* **117B** (1982) 119, *Ibid*, p.123; *Phys. Rev. Lett.* **51** (1983) 1.
- [31] V. Molchonov et al. (SELEX Collaboration), *Phys. Lett.* **B521** (2001) 171.
- [32] D. Berg et al., *Phys. Lett.* **B98** (1981) 119.
- [33] C. Chandlee et al., *Phys. Rev. Lett.* **51**, 168 (1983).
- [34] M. A. Moinester, hep-ph/9410215.
- [35] V. Alexakhine et al., COMPASS GEANT (COMGEANT),  
<http://valexakh.home.cern.ch/valexakh/wwwcomg/index.html>
- [36] A. Akhundov, S. Gerzon, S. Kananov, M.A. Moinester, *Z. Phys.* 66C (1995)279.
- [37] N. I. Starkov et al. *Sov. Jour. Nucl. Phys.* **36**, 1212 (1982).
- [38] A. Sadovski et al., Test beam studies for a trigger for a Primakoff measurement,  
COMPASS collaboration meeting, Oct. 2000, Dubna, Russia.
- [39] B. MacGibbon et al., *Phys. Rev. C*52 (1995) 2097; V. Olmos de Leon, *Eur. Phys. J. A*10 (2001) 207
- [40] H. W. Atherton et al., Precise Measurements of Particle Production by 400 GeV/c Protons on Beryllium Targets, CERN 80-07 Report, 1980.
- [41] M. Benot et al., *Nucl. Instr. Meth.* 105 (1972) 431; C. Bovet, S. Milner, A. Placci, CERN/Lab. II/EA/74-4, (Rev. Aug 1975), The CEDAR Project; Cerenkov Differential counters with Achromatic Ring focus; C. Bovet et al., CERN-SPS/EBP/77-19, The CEDAR Project, *IEEE Trans. Nucl. Sci.* 25 (1978) 572; C. Bovet et al., CERN report CERN 82-13, "The CEDAR counters for particle identification in the SPS secondary beams: a description and operation manual".
- [42] M. Moinester, [http://www-nuclear.tau.ac.il/~murraym/COMPASS/laser\\_monitor\\_techrep.html](http://www-nuclear.tau.ac.il/~murraym/COMPASS/laser_monitor_techrep.html)
- [43] J. Ahrens *et al.*, Measurement of the  $\pi$  Meson Polarizability,  
U. Mainz MAMI A2 Proposal, *Few-Body Suppl.* **9**, 449 (1995).
- [44] C. Unkmeir, U. Mainz, Ph.D. thesis, 2000.
- [45] R. Hicks *et al.*, JLab Proposal E99-010.